Available online at www.sciencedirect.com
ScienceDirect
Journal of the European Ceramic Society 31 (2011) 1957–1963
www.elsevier.com/locate/jeurceramsoc

# Sintering of α-alumina for highly transparent ceramic applications

Johan Petit [a,*], Philippe Dethare [a], Alessandra Sergent [a], Robert Marino [a], Marie-Hélène Ritti [a], Stéphane Landais [b], Jean-Luc Lunel [b], Sandrine Trombert [c]

[a] ONERA, Composite Structures and Materials Department, BP 72, 29 avenue de la Division Leclerc, 92322 Chatillon Cedex, France
[b] ONERA, Metallic Structures and Materials Department, Chemin de la Hunière, 91761 Palaiseau Cedex, France
[c] BAIKOWSKI, Les Marais Noirs ouest, BP501, 74339 La Balme de Sillingy Cedex, France

Received 10 January 2011; received in revised form 15 April 2011; accepted 30 April 2011

**Abstract**

In this paper we present our results on the sintering of α alumina ceramics by hot isostatic pressing. It describes a simple method for obtaining precise relative density values on our almost 100% dense samples. Then, transparency results are discussed with respect to grain size and residual porosity measurements, comparing them to scattering calculations. Our results are not far from the best reported transmission values: almost 60% for a 1 mm thick sample. The other 40% diffuse light comes from the birefringence of alumina for the most part. However, they are transparent enough to see detailed structures at several kilometers through them.


*Keywords:* Hot isostatic pressing; $Al_2O_3$; Optical properties

## 1. Introduction

For some extreme applications of visible-infrared windows, materials like organic polymers, glass or even single crystals are not very appropriate. Polymers are unstable above 200 or 300 °C, types of glass are often too soft in abrasive conditions and single crystals are quite difficult to produce into big pieces. $MgAl_2O_4$ (spinel), $Y_3Al_5O_{12}$ (YAG), α-$Al_2O_3$ (Alumina),[1] are some oxide ceramics which are good candidates for such applications because of their strong thermo-mechanical properties until a very high temperature (>1000 °C) is reached, their intrinsic transparency over the visible-IR range and the low costs of the raw materials. Among those compounds, the one that retains our attention is alumina. Indeed, its flexural strength,[2] hardness,[3] Young's modulus,[4] melting point, fracture toughness[5] are among the highest for oxide compounds. However, the processing of a transparent ceramic is a challenge because its density has to be close to that of a single crystal. If the relative density (which is the ratio between ceramic and crystal densities) is not equal to the one, the sample is not at its maximum transparency. Another source of opacity is the presence of impurities. During the single crystal growth process, the segregation eliminates them. On the contrary, during the sintering process, they stay inside the sample and can form parasitic phases. Finally, in the case of alumina, grain boundary plays a large part in the light scattering.[6] Indeed, because of its birefringence, the random oriented grains of such a ceramic induce a variation of the refractive index along any direction. As it is now well known, the control of the grain growth is essential for improving the transparency of alumina ceramics as well as the densification rate. The problem is that the grain growth is linked to the treatment temperature rather than the treatment time. On the one hand, the thermodynamic energy state of a powder is greater than that of the fully dense ceramic, which is in turn greater than that of the single crystal because of surface energies. However, a powder cannot turn into a dense material if it remains in ambient conditions (considering human time scale). The activation energy is too huge. To improve the kinetics, the ceramist, as often in chemistry, must increase the process temperature and/or use a catalyst. In a solid state medium (so with no convection), the former is much more efficient. An increase of the pressure is also recommended to pass through that energy wall. On the other hand, when the treatment time is decreased enough by increasing the temperature, the grain growth becomes much too important. Sintering aids or grain growth limiters can be added to the ceramics but, in too large quantities, they create

* Corresponding author..
*E-mail address:* johan.petit@onera.fr (J. Petit).

0955-2219/$ – see front matter © 2011 Elsevier Ltd. All rights reserved.
doi:10.1016/j.jeurceramsoc.2011.04.034

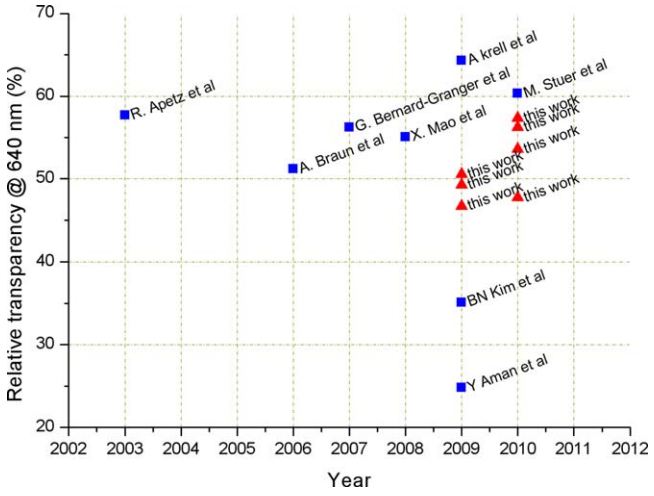


Fig. 1. Changes in alumina ceramics transparency at about 640 nm. Every value is adjusted for a 1 mm thick sample. 100% corresponds to the maximum theoretical transparency value for alumina. Krell et al.[18], Stuer et al.[7], Mao et al.[19], Braun et al.[20], Kim et al.[21], Aman et al.[8], Apetz and Van Bruggen[6], Bernard-Granger and Guizard[22].

parasitic phases. Some authors have chosen the spark plasma sintering (SPS) technique to densify their samples and control the grain growth.[7–9] Here, we used the hot isostatic pressing (HIP) technique. First of all, we will present a brief state of the art of that research topic before outlining the transparency calculus in a polycrystalline alumina. Then, we will present and discuss our experimental results.

## 2. State of the art

In Fig. 1, we show the main published results on transparent polycrystalline alumina. On this graph, 100% represents the maximum theoretical transparency (the maximum absolute transparency is 86% for alumina because of face reflection losses). Scattering or even absorption losses are volumic values. That is why they depend on the sample's thickness. Here, every reported value is converted into a relative transparency for a 1 mm thick sample using Eq. (17). While other compounds like spinel,[10,11] YAG,[12,13] $Y_2O_3$ (yttria)[14,15] or $Lu_2O_3$[16,17] have shown relative transparency close to 100%, it seems, in the case of alumina, researchers and engineers have great difficulty in improving it beyond 60–70%.

Some obtained their best result with pure alumina,[8,18,20] others with doped alumina (MgO or $TiO_2$[22]; $MgO + La_2O_3 + Y_2O_3$[7]) and, finally, some tried to orientate grains.[19] As a comparison, we show our results during the last two years on the same graph (Fig. 1). In that context, our results are not far from the best ones but we are also confronted by the same transparency limit. This can be explained quite simply by discussing the well-known scattering theory. Indeed, supposing there are no absorbing centers, the main scattering comes, on the one hand, from the porosity and, on the other, from the grain boundary because of randomly oriented birefringent alumina grains.

As proposed in,[6] considering grain sizes range from 0.1 to 10 times the visible light wavelengths (about 40 nm to 6 μm), the Rayleigh–Gans–Debye theory can be applied for grain boundary scattering modeling. Thus, the grain boundary scattering coefficient $\gamma_{gb}$ can be written as:

$$\gamma_{gb} = 3\pi^2 r \frac{\overline{\Delta n}^2}{\lambda_0^2} \quad (1)$$

$$\overline{\Delta n} = \frac{2}{3}\Delta n \quad (2)$$

with $r$, the mean grain radius; $\Delta n$, the birefringence; and $\lambda_0$, the light wavelength in the vacuum. Here, we consider that the light passes through many grains along the sample so we must consider the mean refractive index difference between two grains, $\overline{\Delta n}$. The 2/3 coefficient (Eq. (2)) is due to the uniaxial structure of alumina.

Pecharroman et al.[23] suggested another formula for grain boundary scattering:

$$\gamma_{gb} = \langle a \rangle \frac{6\pi^2}{\lambda^2}\Delta n^2 \alpha(\xi) \quad (3)$$

with $\alpha(\xi)$ (see Eq. (4)) the textural function and $\xi$ the textural angle which corresponds to the grain orientation organization of the ceramic. A value of $\xi = 45$ means that all grains are totally randomly distributed.

$$\alpha(\xi) = \frac{(11 - 4\cos(2\xi) + \cos(4\xi))\sin^4(\xi)}{(\cos(2\xi) - 3)^2} \quad (4)$$

$\langle a \rangle$ is the medium radius value corresponding to the volume grain distribution which could be estimated to be the maximum value of experimentally found grain radius in case of heterogeneous grain size distribution according to the authors. They explained that in Eqs. (1) and (2) several mistakes appear which fortunately give results close to experiments.

Consequently, the transmission $T$ with respect to the sample thickness $d$ is expressed as:

$$T_{gb} = \left[1 - \left(\frac{n-1}{n+1}\right)^2\right]^2 e^{-\gamma_{gb}d} \quad \text{(absolute)}$$
$$\text{and} \quad T'_{gb} = e^{-\gamma_{gb}d} \quad \text{(relative)} \quad (5)$$

The pre-exponential factor corresponds to the Fresnel losses (reflection losses) with n the refractive index of the material.

In Fig. 2, we can see that the Pecharroman model is stronger that the Apetz' one. It also shows that at 640 nm (visible light), obtaining a high transparency with alumina ceramics is very difficult because it decreases rapidly with increasing grain size. Here, we can see the "wall" mentioned above of 60–70% corresponds to a pore size of about 500 nm.

It is often reported that the grain boundary scattering (Eq. (5)) is enough to model the transmission curve of fully dense ceramics. Nevertheless, a ceramic is rarely fully dense. Even a fraction of a percent of porosity introduces sensible scattering

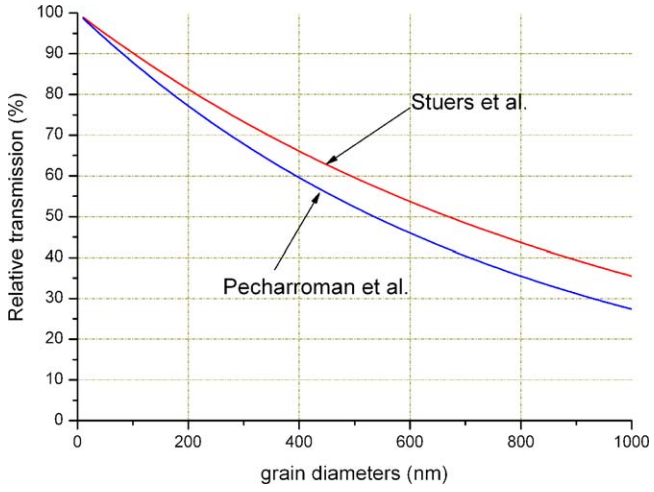


Fig. 2. Relative transmission at 640 nm of a 1 mm thick alumina ceramic sample versus the mean grain size if you consider the Apetz model (Eqs. (1) and (5)); and the maximum observed grain size if you consider the Pecharroman model (Eqs. (3) and (5)).

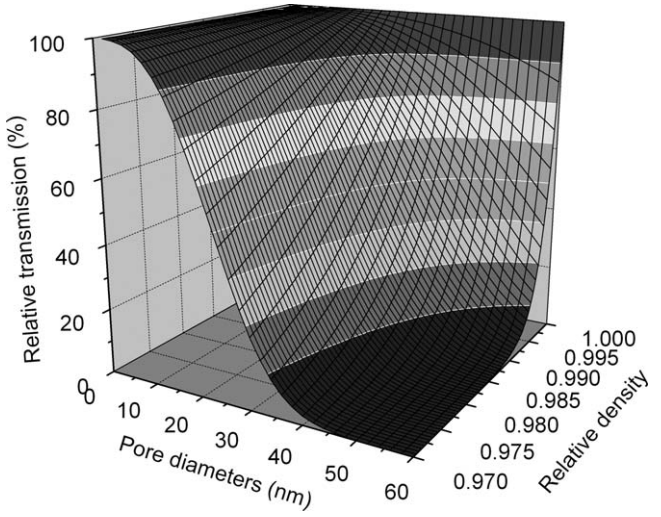


Fig. 3. Relative transmission at 640 nm versus the relative densities and the pore diameters (Eq. (10)). Only the pore's light scattering is considered here. The sample thickness is 1 mm.

losses. To model that part of scattering $\gamma_p$, we can use Schuster's derivation of the Rayleigh formula[24]:

$$\gamma_p = \frac{32\pi^3}{3}\frac{NV^2\mu^2\bar{n}^4}{\lambda^4} \tag{6}$$

with $N$, the pore concentration; $V$, the pore volume; $\bar{n}$, the mean refractive index of the sample; $\lambda$, the vacuum light wavelength; and

$$n_p = \bar{n}(1+\mu) \tag{7}$$

We consider the pore index $n_p$ equal to 1. We can estimate in a totally randomly arranged alumina grain that:

$$\bar{n} = \frac{2n_\perp + n_{//}}{3} \tag{8}$$

$n_\perp$ and $n_{//}$ being the refractive indexes perpendicular and along the optical axis, respectively.

If we call $\tau$ the relative density of the ceramic:

$$N = \frac{1-\tau}{V} \tag{9}$$

Thus, considering only the pore scattering:

$$T_p = \left[1 - \left(\frac{n-1}{n+1}\right)^2\right]^2 e^{-\gamma_p d} \quad \text{(absolute)}$$
$$\text{and} \quad T'_p = e^{-\gamma_p d} \quad \text{(relative)} \tag{10}$$

Fig. 3 is interesting: for a compound with no grain boundary scattering, like in a cubic material (optically isotropic), the pore scattering is very important for a relative density below 99%. That is why researchers try to tend to a fully dense material for transparent ceramic applications. However, it is not a necessary condition. Even at 97% or below highly transparent ceramics can be obtained: the pore radius must be less than about 5 nm. That parameter can be controlled. The pore size is determined by the starting powder grain size and the thermal treatment. To keep it small, a small grain powder (much below 100 nm) and very low temperatures must be used. At low temperature, sintering does not densify powders efficiently, so very high pressures (more than 1 GPa) must be used.[25]

Combining Eqs. (5) and 10, the total transmission (with grain and pore scattering) is:

$$T = \left[1 - \left(\frac{n-1}{n+1}\right)^2\right]^2 e^{-(\gamma_p+\gamma_{gb})d} \quad \text{(absolute)}$$
$$\text{and} \quad T' = e^{-(\gamma_p+\gamma_{gb})d} \quad \text{(relative)} \tag{11}$$

In conclusion, to increase the transparency of the ceramics: the porosity or the pore size must be as low as possible and grains must stay small.

In addition, another parameter can be tuned to increase the transparency in polycrystalline alumina. Although the birefringence, $\Delta n$, is fixed in pure alumina, its average value ($\overline{\Delta n}$ from Eq. (2) or $\Delta n\sqrt{\alpha(\xi)}$ from Eq. (3)) can be reduced. That was the idea of Mao et al.[19] They successfully orientated the ceramic grains using a strong magnetic field of 12 T. It is a very high value and almost impossible for homogenous meter-size samples.

## 3. Experiments

The Baikowski Company supplied directly alumina suspensions, based on ultra-pure alpha alumina synthesized by the alum process. The total impurities did not exceed 100 ppm (K ~ 60 ppm; Na ~ 14 ppm; Si ~ 13 ppm for the most important species). The alumina powder was wet-milled, in order to perfectly de-agglomerated it, and each individual particle had a mean diameter in the range of 100–150 nm – depending on milling parameters – measured by SEM or laser diffraction granulometer (Horiba LA920). The ~75 wt% solid suspension did not contain any organic additive. The suspension was cast

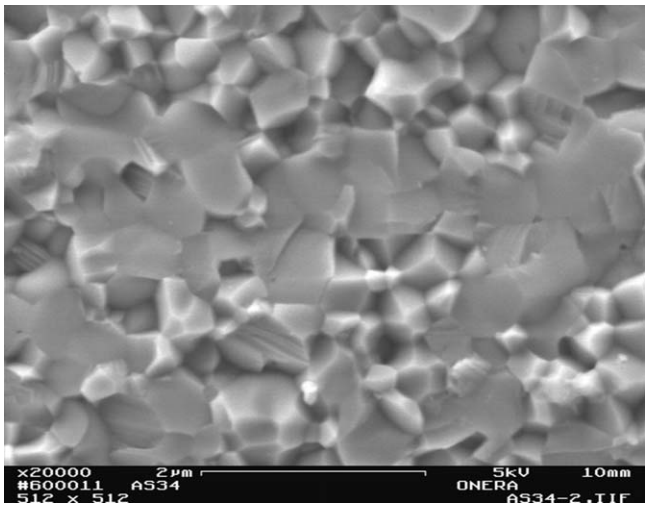


Fig. 4. SEM picture on a HIPed ceramic sample: natural sintering 1200 °C/2 h and HIP 1200 °C/3 h.

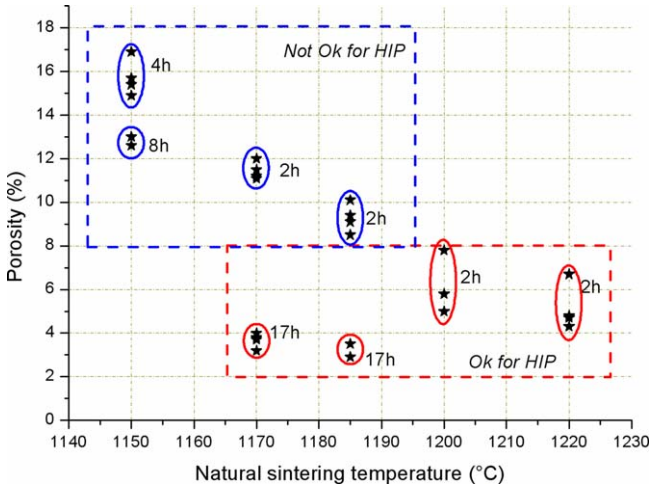


Fig. 5. Total porosity versus the natural sintering temperature. The different treatment times are indicated. The pressure is $\sim 10^{-6}$ mbar.

in a Büchner where we had placed a nylon filter (pore diameter = 0.2 µm). After pulling the liquid across the filter using vacuum for 12 h, green bodies can be easily handled. They were dried at 65 °C for 15 h and then at 600 °C for 30 min under vacuum (<1 mbar). Then, the samples were sintered naturally under vacuum ($10^{-6}$ mbar) around 1200 °C for 2–17 h. Porosity was measured by the Archimedes method considering an alumina single crystal density of 3.96 g cm$^{-3}$. If it was beneath 10%, samples were hot isostatically pressed (HIP) around 1200 °C under 170 MPa of argon during 3–5 h. The furnace employed in the HIP was made of molybdenum. The final relative density after HIP was measured with a very precise method comparing single crystal and ceramic masses outside and inside a liquid (here, it was water). Indeed, the single crystal ($\rho_S$) and ceramic ($\rho_C$) densities are expressed as:

$$\rho_S = \frac{m_S}{V_S} \tag{12}$$

$$\rho_C = \frac{m_C}{V_C} \tag{13}$$

with $m_S$ and $m_C$, the single crystal and ceramic sample masses; $V_S$ and $V_C$ their volume.

When these samples are totally immerged in a liquid like water (density $\rho_w$) their masses $m_{Sw}$ and $m_{Cw}$ can be calculated by:

$$m_{Sw} = m_S - V_S\rho_w \tag{14}$$

$$m_{Cw} = m_C - V_C\rho_w \tag{15}$$

Combining Eqs. (12)–(15), one can find that the relative density $\tau$ is:

$$\tau = \frac{\rho_C}{\rho_S} = \frac{m_C}{m_S} \cdot \frac{m_S - m_{Sw}}{m_C - m_{Cw}} \tag{16}$$

This method is very precise and robust because it takes into account only masses which can be easily measured with high precision. The alumina and water densities which depend on the temperature and their quality disappear.

The grain size was estimated using SEM pictures on fracture planes (see Fig. 4). The method was described in[26]: it is a line intercept method with a correction factor of 1.56 between the measured average grain size on the plane and the one inside the volume.

The transmission curves were measured by a Varian Cary 6000. As previously mentioned, it is important to compare sample transmissions with the same thickness. To correct a transmission $T_{d'}$ obtained with a thickness $d'$ into a transmission $T_d$ for a reference thickness $d$, it is quite easy to find Eq. (17) using Eq. (11):

$$T_d = T_{d'}\left(\frac{T_{d'}}{\left[1 - ((n-1)/(n+1))^2\right]^2}\right)^{(d-d'/d')} \tag{17}$$

## 4. Results

Fig. 5 presents the porosity values of the samples after natural sintering under vacuum versus the treatment temperatures and times. It is well known that, for a constant treatment time, the porosity increases when the temperature decreases. However, under our conditions, we had noticed that above 8% porosity, the HIP treatment is inefficient as presented in Fig. 5. For 1200 °C and 1220 °C, 2 h of dwell are enough. But at 1170 and 1185 °C, we needed to treat them for 17 h to decrease the porosity below 4%.

Furthermore, the treatment temperatures and times also affect the grain size (see Fig. 6): an example of a SEM picture of our ceramic is presented in Fig. 4.

An important thing to notice is that all the samples of this work have quite homogenous grain sizes. We did not notice any suspect grain growth confirming the good quality of the raw materials and the process. The grain size of the starting powder is around 100–150 nm. For treatments at 1200 and 1220 °C, we obtained grains below 400 nm after 2 h of dwell. This size was also found in the 1170 °C treated sample for 17 h. In the contrary, for 17 h at 1185 °C, the grain size is above 600 nm.

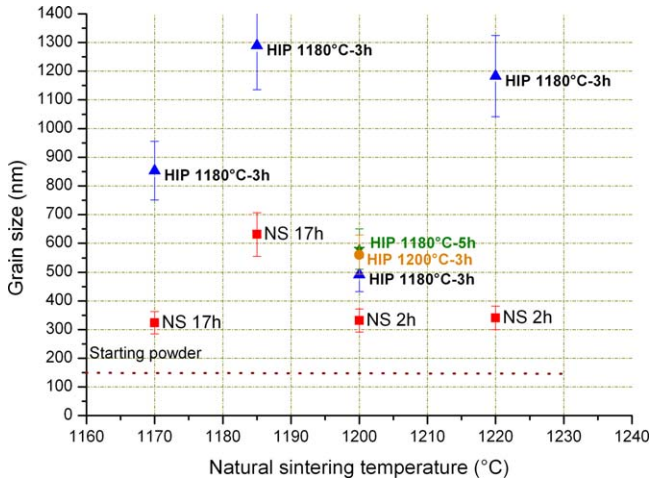


Fig. 6. Grain sizes of ceramics versus the natural sintering (NS) temperature: (square), after natural sintering; (triangle), after HIP at 1180 °C, 170 MPa, 3 h; (disc), after HIP at 1200 °C, 170 MPa, 3 h; (star), after HIP at 1180 °C, 170 MPa, 5 h. The HIPed ceramic values are placed versus the temperature of the corresponding natural sintering.

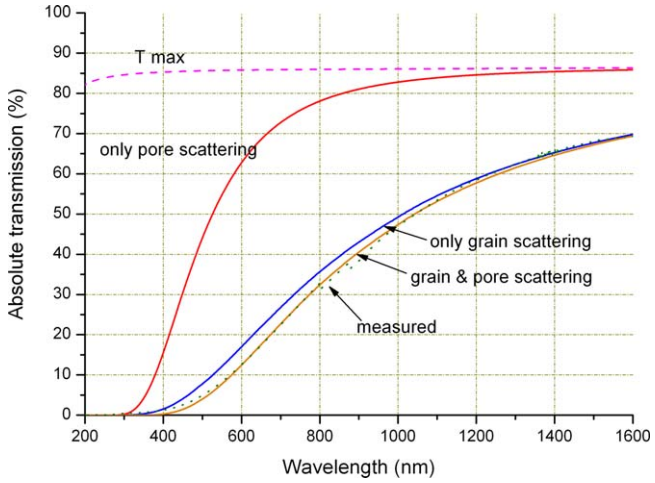


Fig. 8. Comparison between the measured transmission (dashed curve) of a 2.8 mm thick sample (NS 1200 °C/2 h, HIP 1180 °C/5 h) and the calculated ones (solid curves) using Eqs. (5), (10) and (11) according to the Pecharroman et al. model. The calculation parameters are: maximum grain size = 800 nm; pore size = 30 nm, relative density = 0.9986. In Eq. (4), we used $\xi = 35°$.

After the HIP treatment, the grain sizes increase. We can say, approximately, the more it is after the natural sintering, the more it is after HIP sintering. We also tested the HIP conditions on one type of naturally sintered samples (2 h at 1200 °C). As we might suppose, when the temperature or dwell time is increased, the grain sizes increase. However, it is much less obvious than with the natural sintering.

Lastly, we can compare those values to the relative density (Fig. 7). It appears that the natural sintering temperature has also an influence on it. For the same HIP treatment, the higher the natural sintering temperature, the weaker the relative density. It is interesting to note that the samples naturally sintered at 1170 °C and 1185 °C followed by a HIP at 1180 °C for 3 h and the samples sintered at 1200 °C followed by a HIP at 1180 °C for 5 h have an equal relative density (0.9985) but a totally different grain size (between 580 and 1300 nm). Thus, high relative densities can be obtained with a controlled grain growth, even in pure alumina.

Table 1 summarizes the relative densities, grain sizes and relative transparencies of some samples. It is clear that the transmission is linked to the average grain size of the sample and to its residual porosity $(1 - \tau)$. Indeed, we cannot apply a simple correlation between the transmission and the grain size. For example, the 610 nm grain size sample transmits a bit more than the 450 nm one whereas the Rayleigh–Gans–Debye theory (Eqs. (1) and (3)) indicates the contrary. This is the proof that the pore scattering (Eq. (6)) has to be taken into account. That is why we proposed Fig. 8. It shows the experimental transmission curves and the calculated ones from Eqs. (5), (10) and (11) according to the Pecharroman model (Eqs. (3) and (4)). We used the relative density and the grain size shown in Table 1. The pore size was measured on SEM pictures (∼30 nm). The fit was quite good but, to improve it, another parameter had to be changed as reported by C. Pecharroman[23]: instead of a textural angle of 45° as in randomly oriented grains, we used $\xi = 35°$. It can be explained

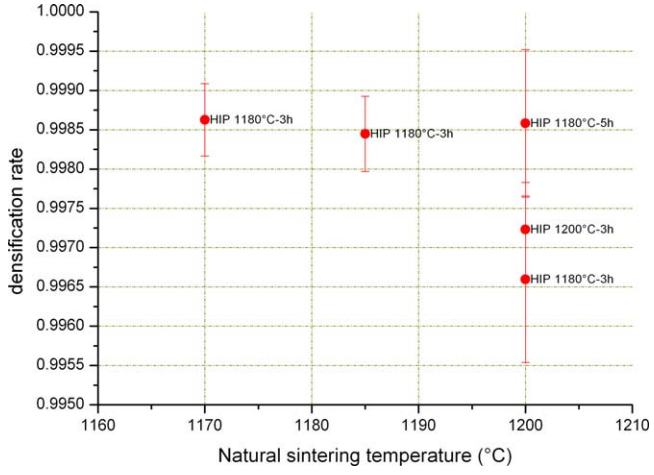


Fig. 7. Relative density ($\tau$) after HIP treatment versus the natural sintering temperature. The HIP parameters are indicated for each data.

Fig. 9. The Eiffel Tower observed through one of our best polycrystalline alumina sample (thickness = 2.8 mm).

Table 1
Summary of the results obtained on some samples. The relative transmission at 640 nm for a 1 mm thick sample is also reported (Fig. 1).

| Natural sintering | HIP | Relative density | Grain size average/max | Transmission at 640 nm for a 1 mm thick sample (%) |
|---|---|---|---|---|
| 1170 °C/17 h | 1180 °C/3 h | 0.9986 | 850/1100 | 54 |
| 1185 °C/17 h | 1180 °C/3 h | 0.9985 | 1290/1600 | 48 |
| 1200 °C/2 h | 1200 °C/3 h | 0.9972 | 560/1200 | 51 |
| 1200 °C/2 h | 1180 °C/3 h | 0.9966 | 490/680 | 56 |
| 1200 °C/2 h | 1180 °C/5 h | 0.9986 | 580/800 | 58 |

in two different ways. On the one hand, this adjustment would be necessary because of our approximations: we did not take into account the grain and pore size distributions and there are errors on grain size determination. But, to find the same curve using $\xi = 45°$, the maximum grain size must be reduced until 400 nm which is totally incompatible with experimental results. On the other hand, during the sintering process, the grains would try to reorient in a common direction to reduce the grain boundary energy. If so, it could be very interesting to find out how to enhance this phenomenon because it is a powerful method to increase the polycrystalline alumina transparency.

So, to increase transmission, not only the grain size must be reduced but also the residual porosity. For HIPed samples, looking at the relative density measured with a method like the one proposed here (Eq. (16)), it appears that few tenths of a percent can affect the optical quality a great deal. To improve the densification, Fig. 7 shows that the natural sintering temperature has to be reduced with a concomitant increase in treatment times. Here, the samples treated at 1170 and 1185 °C are not the most transparent but optimizing the dwell times would probably increase transparency. Moreover, those lower temperatures may keep grain sizes low. Increasing the HIP treatment time also improves densification without affecting the grain size so much. HIP temperature also must be optimized.

Lastly, Fig. 9 shows one of our best results on polycrystalline alumina. As we can see, even at several kilometers, the image is well defined (thickness = 2.8 mm). Nevertheless, it appears dark because of light losses in the visible range. In the IR range the samples are perfectly transparent.

## 5. Conclusion

In this paper, we have described the two main scattering mechanisms, and their well known model, occurring in polycrystalline alumina with submicronic grains. Because of its birefringence, grain boundary scattering is very important but pore scattering is not negligible. Precise relative density measurements showed that even HIPed samples present few tenths of a percent of residual porosity which affects the transparency. With our process consisting of a colloidal dispersion casting, then a natural sintering and, finally, an HIP sintering, we obtained almost 60% of relative transparency which is a very good value. It is enough to observe well resolved pictures at several kilometers across such windows but improvements are still required to decrease the light losses. The grain size is around 600 nm and the residual porosity is around 0.14%. The difference between experimental and calculated transparency curves can be eliminated by reducing the average refractive index difference between two adjacent grains. This could mean they slightly reorganize during the sintering step to minimize the grain boundary energy.

Thank to this process, we obtained homogenous samples in terms of grain size, porosity and transmission. That good point opens the way for large transparent pieces. We are at the beginning of the study and we expect to improve the quality of our windows in the next year by following the directions for research outlined here.

## Acknowledgments

This work is a part of the CERATRANS project. We would like to thank the ANR (French National Research Agency) for its funding support. We also would like to acknowledge Bruno Viana and Philippe Goldner of the LCMCP (UMR CNRS 7574) in Paris, France, for their help in spectroscopy measurements.

## References

1. Light B. Common-aperture IR imaging systems handle multispectral demands. *Laser Focus World* 2010;**October**:55–7.
2. Cho S-J, Yoon K-J, Kim J-J, Kim K-H. Influence of humidity on the flexural strength of alumina. *J Eur Ceram Soc* 2000;**20**:761–4.
3. Krell A. Improved hardness and hierarchic influences on wear in submicron sintered alumina. *Mater Sci Eng* 1996;**A209**:156–63.
4. Asmani M, Kermel C, Leriche A, Ourak M. Influence of porosity on Young's modulus and Poisson's ratio in alumina ceramics. *J Eur Ceram Soc* 2001;**21**:1081–6.
5. Muchtar A, Lim LC. Indentation fracture toughness of high purity submicron alumina. *Acta Mater* 1998;**46**:1683–90.
6. Apetz R, Van Bruggen MPB. Transparent alumina: a light-scattering model. *J Am Ceram Soc* 2003;**86**:480–6.
7. Stuer M, Zhao Z, Aschauer U, Bowen P. Transparent polycrystalline alumina using spark plasma sintering: effect of Mg, Y and La doping. *J Eur Ceram Soc* 2010;**30**:1335–43.
8. Aman Y, Garnier V, Djurado E. Influence of green state processes on the sintering behaviour and the subsequent optical properties of spark plasma sintered alumina. *J Eur Ceram Soc* 2009;**29**:3363–70.
9. Kim B-N, Hiraga K, Morita K, Yoshida H. Spark plasma sintering of transparent alumina. *Scripta Mater* 2007;**57**:607–10.
10. Krell A, Klimke J, Hutzler T. Advanced spinel and sub-μm $Al_2O_3$ for transparent armour applications. *J Eur Ceram Soc* 2009;**29**:275–81.
11. Dericioglu AF, Kagawa Y. Effect of grain boundary microcracking on the light transmittance of sintered transparent $MgAl_2O_4$. *J Eur Ceram Soc* 2003;**23**:951–9.

12. Lu J, Ueda K-I, Yagi H, Yanagitani T, Akiyama Y, Kaminskii AA. Neodymium doped yttrium aluminum garnet ($Y_3Al_5O_{12}$) nanocrystalline ceramics – a new generation of solid state laser and optical materials. *J Alloys Compds* 2002;**341**:220–5.
13. Ikesue A. Polycrystalline Nd:YAG ceramics lasers. *Opt Mater* 2002;**19**:183–7.
14. Jin L, Zhou G, Shimai S, Zhang J, Wang S. $ZrO_2$-doped transparent ceramics via slip casting and vacuum sintering. *J Eur Ceram Soc* 2010;**30**:2139–43.
15. Zhang J, An L, Liu M, Shimai S, Wang S. Sintering of $Yb^{3+}$:$Y_2O_3$ transparent ceramics in hydrogen atmosphere. *J Eur Ceram Soc* 2009;**29**:305–9.
16. Lu J, Takaichi K, Uematsu T, Shirkawa A, Musha M, Ueda K-I, Yagi H, Yanagitani T, Kaminskii AA. Promising ceramic laser material: highly transparent $Nd^{3+}$:$Lu_2O_3$ ceramic. *Appl Phys Lett* 2002;**81**:4324–6.
17. Shi Y, Chen QW, Shi JL. Processing and scintillation properties $Eu^{3+}$ doped $Lu_2O_3$ transparent ceramics. *Opt Mater* 2009;**31**:729–33.
18. Krell A, Klimke J, Hutzler T. Transparent compact ceramics: inherent physical issues. *Opt Mater* 2009;**31**:1144–50.
19. Mao X, Wang S, Shimai S, Guo J. Transparent polycrystalline alumina ceramics with orientated optical axes. *J Am Ceram Soc* 2008;**91**:3431–3.
20. Braun A, Falk G, Clasen R. Transparent polycrystalline alumina ceramic with sub-micrometre microstructure by means of electrophoretic deposition. *Mat-wiss U Werkstofftech* 2006;**37**:293–7.
21. Kim B-N, Hiraga K, Morita K, Yoshida H, Miyazaki T, Kagawa Y. Microstructure and optical properties of transparent alumina. *Acta Mater* 2009;**57**:1319–26.
22. Bernard-Granger G, Guizard C. Influence of MgO or $TiO_2$ doping on the sintering path and on the optical properties of a submicronic alumina material. *Scripta Mater* 2007;**56**:983–6.
23. Pecharroman C, Mata-Osoro G, Antonio Diaz L, Torrecillas R, Moya JS. On the transparency of nanostructured alumina: Rayleigh–Gans model for anisotropic spheres. *Opt Express* 2009;**17**:6899–912.
24. Stewart JQ. Generalizations of the Rayleigh formula for molecular scattering. *JOSA & RSI* 1925;**December**:581–97.
25. Lu TC, Chang XH, Qi JQ, Luo XJ, Wei QM, Zhu S, Sun K, Lian J, Wang LM. Low-temperature high pressure preparation of transparent nanocrystalline $MgAl_2O_4$ ceramics. *Appl Phys Lett* 2006;**88**:213120.
26. Mendelson MI. Average grain size in polycrystalline ceramics. *J Am Ceram Soc* 1969;**52**:443–6.